

Highly Active, Carbon-supported, PdSn Nano-core, Partially Covered with Pt, as Catalysts for Methanol Oxidation

Hui Wang^a, Vladimir Linkov^b, Shan Ji^{b,*}, Wei Zhang^a, Ziqiang Lei^a and Rongfang Wang^{a,b,*}

¹Key Laboratory of Eco-Environment-Related Polymer Materials, Ministry of Education of China, Key Laboratory of Gansu Polymer Materials, College of Chemistry and Chemical Engineering, Northwest Normal University, Lanzhou, 730070, China.

²South African Institute for Advanced Materials Chemistry, University of the Western Cape, Cape Town, 7535, South Africa.

Received 8 December 2011, revised 16 February 2012, accepted 13 March 2012.

ABSTRACT

Carbon-supported, Pt partially covered, PdSn alloy nanoparticles (Pt-PdSn/C) were synthesized *via* a metathetical reaction of PdSn alloy nanoparticles, and a platinum precursor. The electrochemical activity was evaluated by methanol oxidation. The Pt-PdSn/C catalysts were characterized by transmission electron microscopy (TEM), X-ray photoelectron spectroscopy (XPS) and cyclic voltammograms (CV). TEM showed that Pt grows layer-by-layer on the surface of PdSn cores and the thickness of the Pt shell is 0.2 nm, about 1–2 monolayers thick. Cyclic voltammetry results showed that PdSn/C nanoparticles, partially covered by Pt, have a better electrocatalytic performance than conventional PtRu/C and PtPdSn/C catalysts. Electrochemical active surface areas of the Pt-PdSn/C was 2.30 times larger than that of PtRu/C and 1.8 times higher than that of PtPdSn/C catalysts. The results showed that a metathetical reaction is an efficient way of preparing, low Pt loading, highly active electrocatalyst, for methanol oxidation, thus offering great potential for producing Pt-based electrocatalyst for direct methanol fuel cells on a large scale.

KEYWORDS

Electrocatalyst, fuel cell, methanol oxidation, Pt-decorated.

1. Introduction

Platinum-based electrocatalysts are exclusively used for catalyzing oxygen reduction reaction (ORR) and methanol oxidation reaction (MOR) in Direct Methanol Fuel Cells (DMFCs).^{1,2} There are, however, several limitations of Pt-based electrocatalysts, such as high cost, low availability of platinum and irreversibly inactivated by CO-like poisoning species, which restrict the widespread commercialization of DMFCs.^{3,4} It is desirable to develop low-cost catalysts with comparable activity in methanol oxidation reaction and better CO-tolerance for DMFCs. It has been well documented that improving electrochemical activity of Pt by introducing non Pt metals into the catalyst and reducing the Pt loading are effective ways to alleviate the limitations of platinum-based electrocatalysts for DMFCs.^{5–8}

Currently, PtRu alloy catalysts are still considered as the best catalysts for methanol oxidation reaction in DMFCs. Alloying Pt with Ru can significantly enhance the CO-tolerance of Pt.⁹ Although the PtRu alloy catalysts exhibit high activity in MOR, the high cost of Pt and Ru, restrains their widespread application as anode catalysts for DMFCs.¹⁰ Compared to Pt, it has been reported that Pd is a low-cost transition metal with high catalytic activity towards methanol oxidation.¹¹ Although Pd is a promising candidate to replace Pt, the electrochemical activity for MOR still needs to be improved. As a means of improving electrochemical activity of Pd, alloys of various compositions based on Pd have been developed as an alternative to Pt-based electrocatalysts for MOR. In order to further lower the cost and enhance the electrochemical activity, development of tri-metallic catalysts with adding a third low-cost metal, such as Sn, Fe, has also attracted attentions since they result in higher methanol electrooxidation activity and better CO-tolerance.^{12,13}

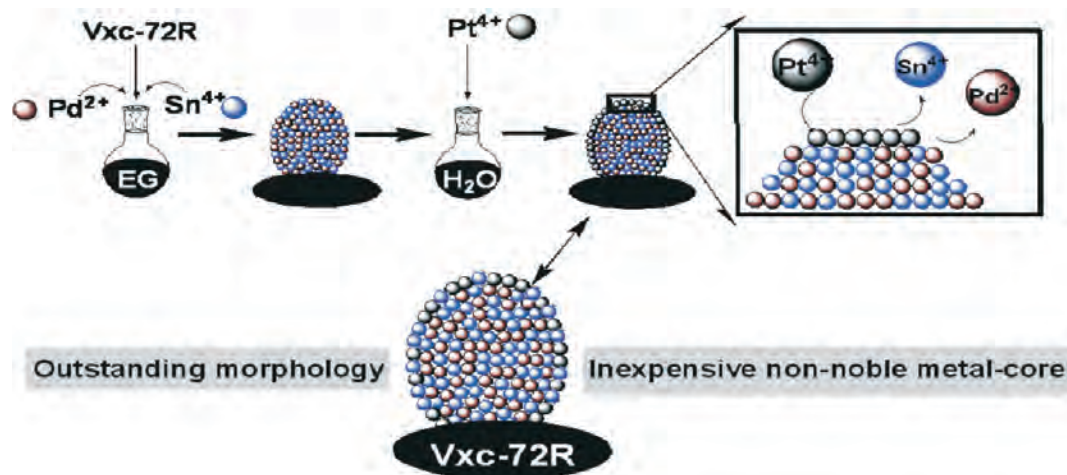
It has been reported that the introduction of metal Sn into Pt/C and Pd/C catalysts can improve the catalytic activity and stability of Pt and Pd toward the electrooxidation of methanol.^{13,15} The presence of Sn can weaken the adsorptive bond of the reactive intermediates, such as CO_{ads} and COOH_{ads}, and easily remove CO-like species by providing oxygen species at low potentials. Sn can also prevent the accumulation of poisoning-intermediates and provide more Pd sites for the direct HCOOH decomposition *via* an direct pathway to CO₂.¹⁶ In addition, a core-shell structure is another efficient way to improve the utilization rate of noble metals and can further lower the cost of the catalyst without sacrificing the electrochemical activity.^{17,18} Tian developed a seed-mediated, growth method, to synthesize core-shell nanoparticles and showed that the electrochemical activity of the nanoparticles started to decrease when the monolayer coverage of Pt on the core was more than 50%.¹⁹ Therefore, it would be beneficial if core-shell structures could be formed with a shell which is partially covered with Pt atoms.

In this work, a facile route for synthesizing carbon-supported, PdSn nano-cores (Pt-PdSn/C), partially covered with Pt, is reported. The highly catalytic active catalysts, with low Pt loading, were prepared *via* metathetical reaction between PdSn alloy nanoparticles (deposited on carbon) and PtCl₄²⁻ solution. This resulted in an architecture, similar to a core-shell structure, which increases the utilization rate of Pt significantly. By this method, the coverage of Pt on the core can be tailored by the atomic ratio of the core alloy. The morphological properties and electrochemical behaviour of the synthesized catalysts were investigated.

2. Experimental

Pt-PdSn/C catalysts were prepared by a two-step method. Firstly, the PdSn/C catalyst with a nominal atomic ratio

* To whom correspondence should be addressed.
E-mail: sji@uwc.ac.za (S.J.) / wrf38745779@26.com (R.W.)



Scheme 1

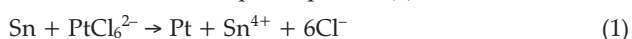
Synthesis of Pt-PdSn/C catalyst using a sequential reduction process.

Pd:Sn = 1:1 was prepared as follows: palladium chloride (PdCl_2), stannic chloride pentahydrate ($\text{SnCl}_4 \cdot 5\text{H}_2\text{O}$) and sodium citrate were dissolved in ethylene glycol (EG) and stirred for 0.5 h. Pretreated carbon black Vulcan XC-72R was added to the above mixture with stirring. The pH of the system was adjusted to ~ 10 using a 5 wt % KOH/EG solution while stirring vigorously. The mixture was then placed into a flask and heated at 160°C for 8 h. The synthesized PdSn/C was filtered, rinsed with deionized water 10 times, and dried in air at 60°C for 5 h. For comparison, PdSnPt/C and PtRu/C samples were prepared by using the same procedure. Secondly, appropriate amounts of $\text{H}_2\text{PtCl}_6 \cdot 6\text{H}_2\text{O}$ and deionized water were added to an empty flask. The obtained PdSn/C powder was transferred into a flask and the mixture stirred at 80°C for 4 h. The synthesized Pt-PdSn/C catalyst was collected by filtration and washed with deionized water to remove chloride anions from the filtrate. The product was dried in air at 60°C for 5 h. A Pt-PdSn/C catalyst, with a nominal atomic ratio Pt:Pd:Sn = 1.0:3.5:3.5, was thus obtained.

TEM measurements were carried out on a Tecnai G220 S-TWIN (FEI Company), using an acceleration voltage of 200 kV. The average chemical compositions of the Pt-PdSn/C catalyst was determined using ICP-AES system (Thermo, U.S.A.). X-ray photoelectron spectroscopy (XPS) (Thi-5702, U.S.A.) was carried out using a monochromatic Al $K\alpha$ X-ray source ($h\nu = 29.35\text{ eV}$). Electrochemical measurements were carried out using an electrochemical workstation (RST). A common three-electrode electrochemical cell was used for the measurements. The counter and reference electrodes were a platinum wire and an Ag/AgCl (3 M KCl) electrode, respectively. The working electrode was a glassy carbon disc (5 mm in diameter).

3. Results and Discussion

Scheme 1 illustrates the synthesis route of carbon-supported Pt-PdSn nanoparticles. The standard reduction potential of $\text{PtCl}_6^{2-}/\text{Pt}$ redox couple ($0.735\text{ V vs. the standard hydrogen electrode (SHE)}$) is much higher than that of the Sn^{4+}/Sn redox couple (0.010 V vs. SHE), while Pd^{2+}/Pd redox couple are $+0.620\text{ V vs. SHE}$. The Sn atoms on the surface of PdSn alloy can be easily oxidized to Sn^{4+} when H_2PtCl_6 solution is added. Theoretically, the Sn atoms on the surface of PdSn nano-cores should react completely with H_2PtCl_6 on the basis of the stoichiometric relationship in Equation (1).



As this metathetical reaction occurs, the Pt atoms are reduced

and deposited on the surface of PdSn nano-cores, instead of independent Pt particles being deposited on the carbon support in the conventional Pt/C catalysts. Due to the intimate interaction between Pt and metal of cores, the Pt particles immobilize on the metal cores are much stable than the Pt particles deposited on the carbon.²⁰ Since there is only a small lattice mismatch of 0.77 % between Pt and Pd metals,¹⁹ the Pt nanoparticles can be easily formed on the top of external Pd layers. After Pt atoms were deposited on the PdSn nano-cores *via* metathetical reaction, the catalyst would be Pt-rich on its surface. New Pt nuclei are not energetically favourable to form in the solution phase according to the new mechanism proposed by Finke-Watzky,²¹ so the reduction of Pt is most likely to occur on the surface of PdSn alloy particles and few monometallic Pt nanoparticles are formed in the solution. The composition of the catalysts was evaluated by ICP-AES analysis and the ratio of Pt:Pd:Sn is 1:3.1:3.8 (atomic ratio), which is close to the ratio of Pt, Pd and Sn precursors. This ratio further proves that most of Pt particles are formed on the surface of PdSn particles, not in the solution.

Typical TEM images for the PdSn/C and Pt-PdSn/C catalysts are shown in Fig. 1a and Fig. 1b. It can be seen that the nanoparticles are deposited onto the carbon with high dispersion and have an irregular polyhedral shape. The size distribution of PdSn/C and Pt-PdSn/C is narrow, mainly in the range of 4–9 nm with the average particle sizes of 6.0 nm and 6.1 nm, respectively. The sizes of Pt-PdSn/C and PdSn/C in the TEM images show similar size and morphology. The atomic radius, cohesive energy and electronegativity of the core and shell metals are the three key factors of whether the mode of growth of shell metal is epitaxial or island one. In the seed-mediated method,^{22,23} Pt in general prefers to form a core-shell cluster structure on the surface of Pd cores. The sizes of Pt-PdSn/C and PdSn/C in the TEM images show similar size and morphology, which indicated that Pt grow layer-by-layer on the PdSn core *via* metathetical reaction. The products were further characterized by HRTEM, as shown in Fig. 1c and Fig. 1d for the PdSn/C and Pt-PdSn/C catalysts. If Pt layers are formed on the surface of PdSn nano-cores, different lattice spacing of external and core layers can be observed in high-resolution TEM (HRTEM), which is a straightforward proof of the layered structure.²⁴ Figure 1c shows that the catalysts are polycrystals, whose lattice spacing (0.218 nm) is close to the value for metallic Pd (111) (0.225 nm), indicating a lattice contraction due to alloying with Sn. Figure 1d presents the HRTEM image of the Pt-PdSn/C catalyst. The measured distance between the two nearest rows is

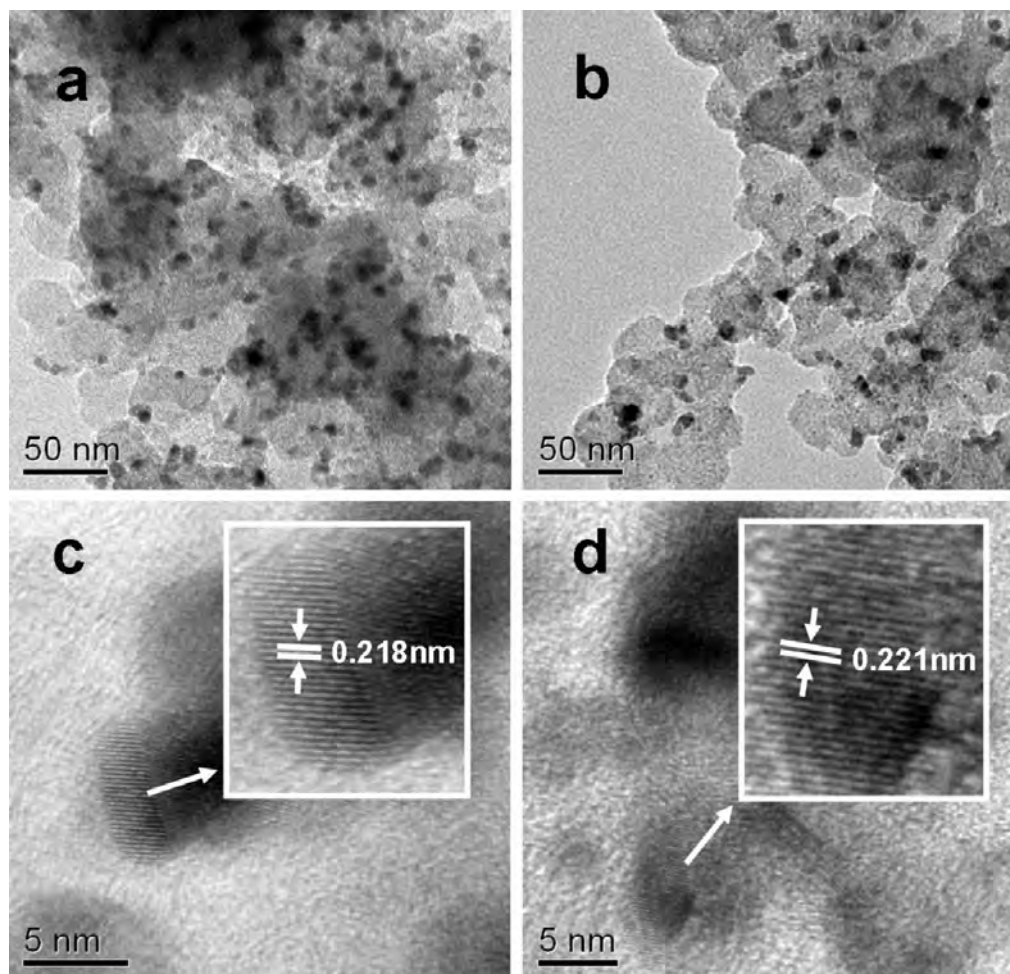


Figure 1 TEM images of (a) PdSn/C and (b) Pt-PdSn/C, and HRTEM images of (c) PdSn/C and (d) Pt-PdSn/C.

0.221 nm, and is smaller than the value for metallic Pt (111) (0.233 nm). This suggests that the Pt shell is formed on the surface of the Sn, and Pt and Sn are alloyed with each other, resulting in lattice contraction. Using the shell model of Schmid,²⁵ and taking into account the precision of the TEM measurements, it is found that the thickness of the Pt shell of the Pt-PdSn/C nanoparticles is 0.2 nm, about 1–2 monolayers thick, which is the Pt coverage found to yield optimal catalytic activity.²⁶

XPS analysis was used to determine the valence state and the surface composition of the as-synthesized catalysts. Figure 2a shows the regional Pt4f spectra of the Pt/C and Pt-PdSn/C samples. The Pt4f spectra shows a doublet containing a low energy band (Pt4f_{7/2}) and a high energy band (Pt4f_{5/2}) at 71.37 and 74.37 eV for Pt/C, and 70.88 and 74.25 eV for Pt-PdSn/C, respectively. Compared to Pt/C there is a negative shift in the binding energies for Pt-PdSn/C, which results from charge transfer from Pd and Sn atoms to Pt atoms. Figure 2b shows that the Pt 4f region of the Pt-PdSn/C displayed as three separate doublets. The doublet (at 70.88 and 74.25 eV), with highest intensity, is a signature of Pt in the zero valent state. The weaker doublets, with binding energies of 1.4 eV higher than Pt(0), are assigned to the Pt(II) oxidation state as in PtO and Pt(OH)₂.^{27,28,29} The third doublet, which is the weakest in intensity with higher binding energies, is most likely caused by a small amount of Pt (IV) residue on the surface.³⁰ A comparison of the relative areas of integrated intensity of Pt(0), Pt(II), and Pt(IV) showed that 68 % of the surface area of the Pt-PdSn/C was covered by metallic Pt.

The cyclic voltammograms (CV) of the PtRu/C, PtPdSn/C and Pt-PdSn/C were carried out in 0.5 M H₂SO₄ solution under N₂ atmosphere and are presented in Fig. 3. All catalysts clearly exhibit the characteristic features of polycrystalline Pt, i.e. hydrogen adsorption/desorption peaks, oxide formation/stripping wave/peak, and a flat double layer region in between. CV was used to calculate the electrochemical active surface areas (ECSA) of the different catalysts. In Fig. 3, the cathodic and anodic peaks appearing between –0.20 and 0.10 V originate from the adsorption and desorption of atomic hydrogen in acidic media. Thus the area of H-adsorption or H-desorption on the CV curve can be used to estimate the ECSA of Pt catalysts.^{31–33} By using the charge passed for H-desorption Q_H , ECSA can be calculated according to the following equation:

$$\text{ECSA (m}^2 \text{ g}^{-1}) = Q_H / (2.1 \times [\text{Pt}]) \quad (2)$$

Here, [Pt] represents the platinum loading (g m⁻²) in the electrode, and 2.1 (C m⁻²) is the charge required to oxidize a monolayer of H₂ on a Pt. The ECSA of Pt-PdSn/C is 71.28 m² gPt⁻¹, which is 2.30 times larger than that of the PtRu/C (30.98 m² gPt⁻¹) catalyst and 1.80 times larger than that of the PtPdSn/C (40.67 m² gPt⁻¹) catalyst. The high ECSA of Pt-PdSn/C may originate from the more exposed, active Pt atoms, on the surface of the Pt-PdSn/C nanoparticles. These exposed Pt atoms maybe responsible for the good electrochemical catalytic performance of the catalyst.

Figure 4 shows the cyclic voltammograms of PtRu/C, PtPdSn/C and Pt-PdSn/C catalysts recorded in 0.5 M CH₃OH + 0.5 M H₂SO₄ aqueous solution. Although onset potentials of three

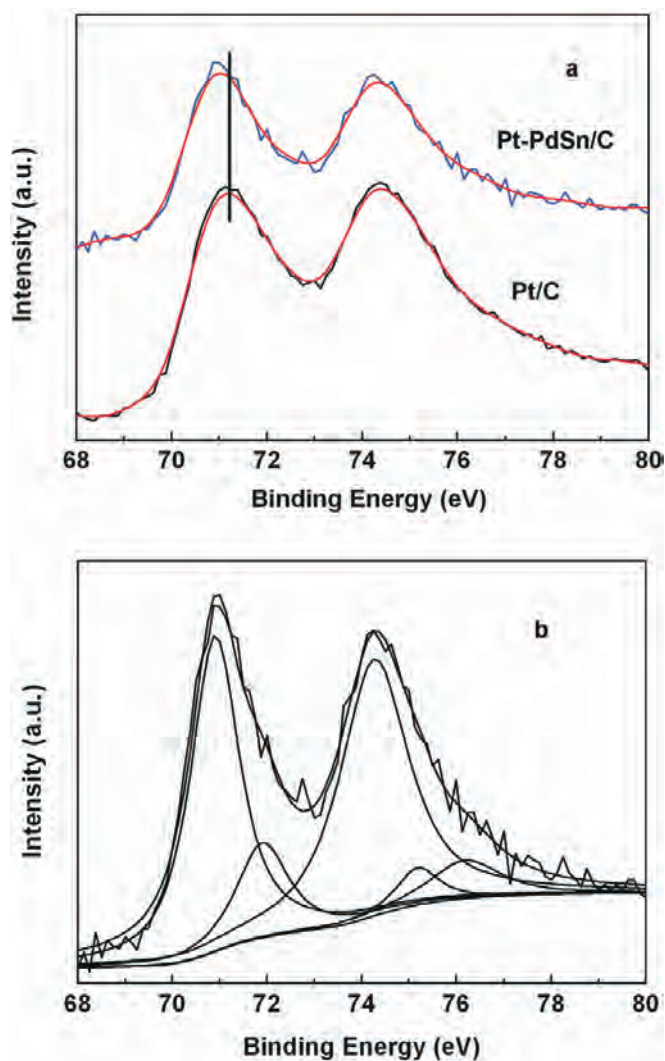


Figure 2 (a) Pt 4f XPS spectra of Pt/C and Pt-PdSn/C catalysts. (b) Pt 4f XPS spectra of the Pt-PdSn/C catalyst fitted with three pairs of overlapping Lorentzian curves.

catalysts are similar, the peak current density of Pt-PdSn/C reaches $0.572 \text{ A mgPt}^{-1}$ at 0.593 V during positive potential scanning process is much higher than that of PtRu/C catalyst

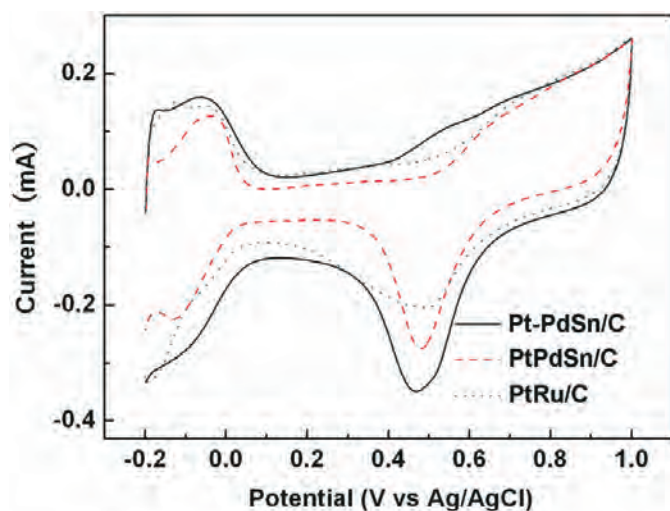


Figure 3 Cyclic voltammograms of PtRu/C, PtPdSn/C and Pt-PdSn/C catalysts in $0.5 \text{ M H}_2\text{SO}_4$ solution under N_2 atmosphere; scan rate = 50 mV s^{-1} ; at $20 \pm 5 \text{ }^\circ\text{C}$.

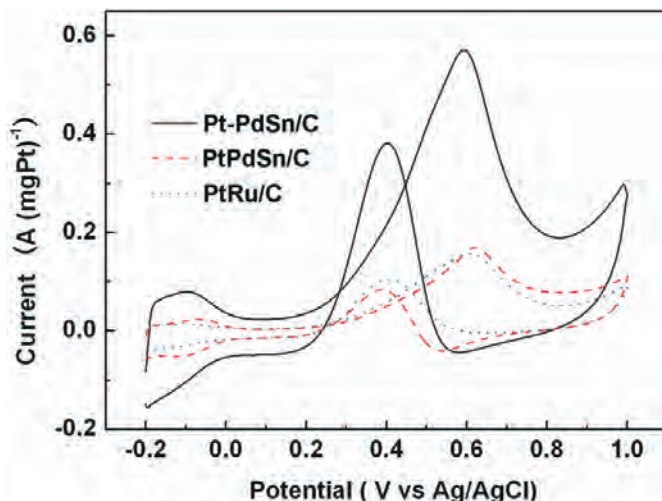
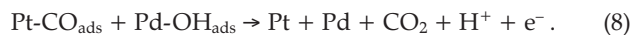
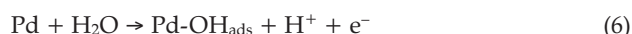
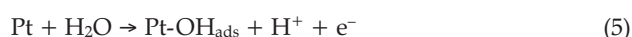
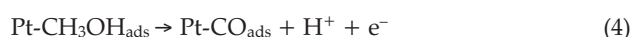


Figure 4 Cyclic voltammograms of PtRu/C, PtPdSn/C and Pt-PdSn/C catalysts in $0.5 \text{ M CH}_3\text{OH} + 0.5 \text{ M H}_2\text{SO}_4$ solution under N_2 atmosphere; scan rate: 50 mV s^{-1} ; at $20 \pm 5 \text{ }^\circ\text{C}$.

($0.157 \text{ A mgPt}^{-1}$ at 0.606 V) and PtPdSn/C ($0.169 \text{ A mgPt}^{-1}$ at 0.620 V) catalyst, which indicate the activity towards methanol electrooxidation for Pt-PdSn/C catalyst is obviously better than PtRu/C and PtPdSn/C catalysts.

In addition, the ratio of the forward oxidation current peak (I_f) to the reverse current peak (I_b), I_f/I_b , is an important index of the catalyst tolerance to the poisoning species.^{4,41–43} A higher ratio indicates more effective removal of the poisoning species on the catalyst surface. Based on the curves in Fig. 4, the I_f/I_b ratio of Pt-PdSn/C is 1.50, which is higher than that of the PtRu/C catalysts (~ 1.20) and PtPdSn/C catalysts (~ 1.32), which shows the best poison tolerance among these three catalysts.

In order to explain the effect of Pd and Sn, a reaction mechanism is proposed in this work. This reaction mechanism is based upon the simplified dual path mechanism accepted for the oxidation of methanol.^{34,35} The mechanism for methanol oxidation on the Pt-PdSn/C catalyst can be presented as follows:



Reactions (3) and (4) occur primarily at the Pt active sites. The zero valent tin atoms change the adsorption properties of Pt, resulting in stronger adsorption of H_2O , presumably in the form of OH. Reaction (5) is then promoted, and leads to an enhancement of methanol oxidation rate.^{36,37} The general theory of bifunctional methanol oxidation mechanism is as follows: Pd is responsible for the water dehydrogenation to form Pd-OH, in other words, reaction (6) occurs, then the reaction of Pd-OH and Pt-CO produces CO_2 and regenerates the active metal on the surface. Without Pd, the water dehydrogenation on Pt will occur at a higher potential, making the overall oxidation process on pure Pt sluggish.³⁸ Taking account of these two factors, reaction (4) would mainly affect the methanol oxidation rate in the low potential. As evidenced from the XPS data, the charge transfer from Pd and Sn to Pt in the core-shell system, causes a substantial increase in electron density around Pt-sites resulting in a weaker chemisorption of CO, which could promote the

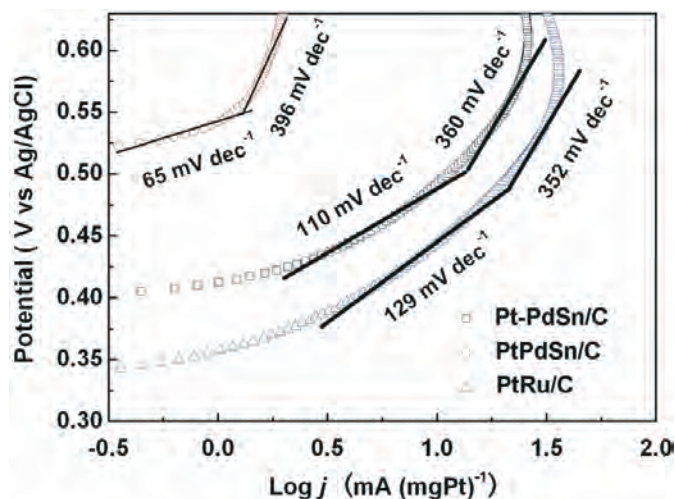


Fig. 5 Tafel plots of MOR on PtRu/C, PtPdSn/C and Pt-PdSn/C catalysts, in 0.5 M CH₃OH + 0.5 M H₂SO₄ solution under N₂ atmosphere. Scan rate: 1 mV s⁻¹.

reactions (6) and (7).^{39,40} The mechanism by which the introduction of PdSn can improve the activity towards methanol oxidation should be considered as a multifunctional effect of the PdSn core and the Pt shell.

In order to further compare the activity towards methanol oxidation of PtRu/C, PtPdSn/C and Pt-PdSn/C catalysts and testify the above mechanism, Tafel slope and exchange current density were carried out for these three catalysts. Tafel plots of the MOR on the PtRu/C, PdSnPt/C and Pt-PdSn/C catalysts, derived from the linear sweep voltammograms in 0.5 M H₂SO₄ + 0.5 M CH₃OH aqueous solution, at a scanning rate of 1 mV s⁻¹, are shown in Fig. 5. Tafel plots can be fitted and divided into two linear regions for all samples, indicating a change in the mechanism or at least a change in the predominance of certain processes. For all catalysts, the fitted Tafel slopes are about 65–129 mV dec⁻¹ at low potentials and about 352–396 mV dec⁻¹ at high potentials. The difference of the Tafel slope values at low and high overpotentials may indicate a possible change of reaction mechanism, or at least a transformation of rate-determining step at different potential ranges. From kinetic theory point of view, it can be concluded that a splitting of the first C-H bond of CH₃OH molecule with the first electron transfer is the rate-determining step of methanol electrooxidation. The result is consistent with the above mechanism. The change of the Tafel slopes at high potentials may be attributed to the insufficient compensation of methanol oxidation for the rapid oxidation reaction on the electrode surface, and the mass transfer of methanol at high potential becomes the rate-determining step.⁴¹ The Tafel slope values in different potential regions reveal that the mechanism and rate-determining step in methanol electrooxidation varies with potential. In the low potential range, methanol dehydrogenation, is the rate-determining step, while in the high potential range, the oxidation and removal of CO_{ads} becomes the rate-determining step. Meanwhile, at intermediate potential, the rate-determining step of methanol electrooxidation is perhaps in the transition range.³¹

4. Conclusions

A carbon-supported Pt partially covered PdSn alloy nanoparticles with low Pt loading were successfully synthesized *via* metathetical reaction of PdSn alloy nanoparticles and platinum precursor. The synthesized Pt-PdSn/C catalyst was characterized by various techniques including TEM, XPS and CV. TEM

showed that 1–2 monolayers of Pt atoms were formed on the surface of PdSn core particles. Electrochemical results prove that Pt-PdSn/C, with low Pt loading, prepared *via* a metathetical reaction, can significantly improve the electrochemical performance and electrochemical active surface areas of Pt-PdSn/C are much higher than that of conventional PtRu/C and PtPdSn/C catalysts. The new method of preparing Pt-based electrocatalyst *via* metathetical reaction has great potential for producing highly active electrocatalysts for methanol oxidation.

Acknowledgements

The authors would like to thank the State Natural Science Foundation of China (21163018), the Postdoctoral Science Foundation of China (20110490847) and the South African NRF (SUR2008060900021) for financially supporting this work.

References

- 1 A. Sarkar, A.V. Murugan and A. Manthiram, *J. Mater. Chem.*, 2009, **19**, 159–165.
- 2 N. Kristian, Y. Yan and X. Wang, *Chem. Commun.*, 2008, **353**, 353–355.
- 3 E. Antolini, J.R.C. Salgado and E.R. Gonzalez, *J. Power Sources*, 2006, **160**, 957–968.
- 4 W. Wang, R. Wang, S. Ji, H. Feng, H. Wang and Z. Lei, *J. Power Sources*, 2010, **195**, 3498–3503.
- 5 H. Li, G. Sun, L. Cao, L. Jiang and Q. Xin, *Electrochim. Acta*, 2007, **52**, 6622–6629.
- 6 J. Otom, S. Nishida, H. Takahashi and H. Nagamoto, *J. Electroanal. Chem.*, 2008, **615**, 84–90.
- 7 A. Caillard, C. Coutanceau, P. Brault, J. Mathias and J.M. Leger, *J. Power Sources*, 2008, **162**, 66–73.
- 8 V. Neburchilov and H. Wang, *J. Zhang, Electrochem. Commun.*, 2007, **9**, 1788–1792.
- 9 M.K. Jeon, K.R. Lee, H. Daimon, A. Nakahara and S.I. Woo, *Catal. Today*, 2008, **132**, 123–126.
- 10 T. Huang, J. Liu, R. Li, W. Cai and A. Yu, *Electrochem. Commun.*, 2009, **11**, 643–646.
- 11 Y. Wang, X. Wang and C.M. Li, *Applied Catalysis B: Environmental*, 2010, **99**, 229–234.
- 12 H. Daimon and Y. Kurobe, *Catal. Today*, 2006, **111**, 182–190.
- 13 S. Pasupathi and V. Tricoli, *Electrochem. Solid-State Lett.*, 2006, **9**, A167–A170.
- 14 D. Tu, B. Wu, B. Wang, C. Deng and Y. Gao, *Applied Catalysis B: Environmental*, 2011, **103**, 163–168.
- 15 D.H. Lim, D.H. Choi, W.D. Lee, D.R. Park and H.I. Lee, *Electrochem. Solid State Lett.*, 2007, **10**, B87–B90.
- 16 Z. Liu and X. Zhang, *Electrochem. Commun.*, 2009, **11**, 1667–1670.
- 17 L. Luo, D. Wang, P.N. Mott, Y. Njoki, T. Lin, Z. He, B.N. Xu, I.S. Wanjana, C. Lim and J. Zhong, *J. Adv. Mater.*, 2008, **20**, 4342–4347.
- 18 N. Kristian, X. Wang, *Electrochem. Commun.*, 2008, **10**, 12–15.
- 19 P. Fang, S. Duan, X. Lin, J.R. Anema, J. Li, O. Buriez, Y. Ding, F. Fan, D. Wu, B. Ren, Z. Wang, C. Amatore and Z. Tian, *Chem. Sci.*, 2011, **2**, 531–539.
- 20 W. Wang, R.F. Wang, S. Ji, H.Q. Feng, Z.Q. Wang and J. Lei, *Power Sources*, 2010, **195**, 3498.
- 21 M.A. Watzky and R.G. Finke, *J. Am. Chem. Soc.*, 1997, **119**, 10382–10400.
- 22 F. Fan, D. Liu, Y. Wu, S. Duan, Z. Xie, Z. Jiang and Z. Tian, *J. Am. Chem. Soc.*, 2008, **130**, 6949–6951.
- 23 J. Hu, J. Li, B. Ren, D. Wu, S. Sun and Z. Tian, *J. Phys. Chem. C*, 2007, **111**, 1105–1112.
- 24 O. Holderer, T. Epicier, C. Esnouf and G. Fuchs, *J. Phys. Chem. B*, 2003, **107**, 1723–1726.
- 25 G. Schmid, *Chem. Rev.*, 1992, **92**, 1709–1727.
- 26 S. Alayoglu, A.U. Nilekar, M. Mavrikakis and B. Eichhorn, *Nature*, 2008, **7**, 333–338.
- 27 J. Zhu, F. Cheng and Z. Tao, *J. Chem. Phys. Chem. C*, 2008, **112**, 6337–6345.

- 28 J. W. Guo, T.S. Zhao, J. Prabhuram, R. Chen and C.W. Wong, *Electrochim. Acta*, 2005, **51**, 754–763.
- 29 F. Liu, J.Y. Lee and W.J. Zhou, *J. Phys. Chem. B*, 2004, **108**, 17959–17963.
- 30 Z.Q. Tian, S.P. Jiang, Y.M. Liang and P.K. Shen, *J. Phys. Chem. B*, 2006, **110**, 5343–5350.
- 31 J. Perez, E.R. Gonzalez and E.A. Ticianelli, *Electrochim. Acta*, 1998, **44**, 1329–1339.
- 32 A. Pozio, M.D. Francesco, A. Cemmi, F. Cardellini and L. Giorgi, *J. Power Sources*, 2002, **105**, 13–19.
- 33 F.B. Su, C.K. Poh, Z.Q. Tian, G.W. Xu, G.Y. Koh, Z. Wang, Z.L. Liu and J.Y. Lin, *Energy Fuels* 2010, **24**, 3727–3732.
- 34 T.H.M. Housmans and M.T.M. Koper, *J. Phys. Chem. B*, 2003, **107**, 8557–8567.
- 35 K. Wang, H.A. Gasteiger, N.M. Markovic and P.N. Ross, *Electrochim. Acta*, 1996, **41**, 2587–2593.
- 36 E. Antolini and E.R. Gonzalez, *Electrochim. Acta* 2010, **56**, 1–14.
- 37 C. Panja, N. Saliba and B.E. Koel, *Surf. Sci.*, 1998, **395**, 248–259.
- 38 Y. Liu, M. Chi, V. Mazumder, K.L. More, S. Soled, J.D. Henao and S. Sun. *Chem. Mater.*, 2011, in press (doi: 10.1021/cm2014785).
- 39 F. Kadirgan, S. Beyhan and T. Atilan, *Int. J. Hydrogen Energy*, 2009, **34**, 4312–4320.
- 40 K. Shukla, A.S. Aricò, K.M. El-Khatib, H. Kim, P.L. Antomucci and V. Antomucci, *Appl. Sur. Sci.*, 1999, **137**, 20–29.
- 41 Y.J. Kim, W.H. Hong, S.I. Woo and H.K. Lee, *J. Power Sources*, 2006, **159**, 491–500.